



# Numerical and Experimental Investigation for Application of CoNiCrAlY Coatings by HVAF

K. Bobzin<sup>1</sup> · H. Heinemann<sup>1</sup> · K. Jasutyn<sup>1</sup>

Submitted: 10 August 2023 / in revised form: 3 January 2024 / Accepted: 4 January 2024 / Published online: 7 February 2024  
© The Author(s) 2024

**Abstract** A relatively small change in oxide content and microstructure in MCrAlY coatings (M = Co, Ni) can affect the functionality of the coating for oxidation protection or as a bond coat. The objective of this study is to fabricate a CoNiCrAlY coating with low porosity and low oxide content. The high velocity air-fuel (HVAF) process, with its relatively low process temperature, is particularly suitable for the deposition of spray materials that are susceptible to oxidation or degradation at high temperature. A CFD simulation model of HVAF process is developed to determine the process parameters for fabricating CoNiCrAlY coating. The simulation results are validated by particle diagnostics, thereby establishing a comprehensive understanding of the underlying process. To assess the coating microstructure, XRD and EDS analyses as well as observation of cross sections of the coatings are conducted. The results highlight the influence of various factors, such as the variation of carrier gas and particle size distribution, on the quality of the coatings. Consequently, the utilization of simulation-based process parameter development is well supported by the coating fabrications, offering valuable insights into the processes prior to implementation.

**Keywords** CFD simulation · coating microstructure · CoNiCrAlY · HVAF · oxide content

## List of Symbols

$A_p$  Surface area of the particle  
 $C_D$  Drag coefficient

$c_p$  Specific heat capacity  
 $d$  Diameter  
 $d_s$  Stand-off distance  
 $F_D$  Drag force  
 $h$  Convective heat transfer  
 $m_p$  Mass of the particle  
 $Nu_p$  Particle Nusselt number  
 $Pr_g$  Gas Prandtl number  
 $Ra$  Surface roughness  
 $Re_p$  Particle Reynolds number  
 $v_g$  Velocity of the gas  
 $v_p$  Velocity of the particle  
 $\kappa_g$  Thermal conductivity of the gas  
 $\rho_g$  Density of the gas

## Introduction

Thermally sprayed MCrAlY coatings, where M represents nickel, cobalt or their combination, are often used as a single-layer coating for oxidation protection or as a bond coat for thermal barrier coatings (TBC) on the turbine blade. During operation, the elements of the coating oxidize and form an oxide layer (thermally grown oxide, TGO) on the surface of the MCrAlY coating or at the interface between the MCrAlY coating and the TBC. The functionality of the coating depends significantly on the oxide content and the microstructure of the MCrAlY coating (Ref 1). Various thermal spraying processes have been investigated to examine the oxidation resistance of CoNiCrAlY bond coat for TBC applications. These include atmospheric plasma spraying (APS), vacuum plasma spraying (VPS), high velocity oxygen-fuel (HVOF) and cold gas spraying (CGS) (Ref 2), each with its own advantages and disadvantages.

✉ K. Jasutyn  
jasutyn@iot.rwth-aachen.de

<sup>1</sup> Surface Engineering Institute (IOT), RWTH Aachen University, Kackertstr. 15, 52072 Aachen, Germany

VPS is cost intensive due to vacuum chamber usage. High process temperatures in APS can lead to excessive oxidation and Al loss in coatings, potentially causing premature MCrAlY failure (Ref 3). During oxidation test, Al in the bond coat formed a protective oxide scale, and some reacted with Ni to create small Al-rich precipitates scattered throughout the bond coat (Ref 4). Coatings with low porosity, comparable to low-pressure plasma spraying coatings, and with oxygen content comparable to good HVOF coatings were prepared using APS and a high velocity nozzle (Ref 5). Coatings with low surface roughness ( $R_a < 6 \mu\text{m}$ ), low porosity, and relatively high oxide content were fabricated by supersonic plasma spraying due to higher particle velocity and axial injection (Ref 6). The HVOF and CGS processes also operate at atmospheric pressure, with lower particle temperatures than APS. CGS results in solid-state particles, leading to minimal oxide content. However, its lower temperature can hinder deformability upon impact, potentially causing porosity and negatively affecting coating properties. CGS-sprayed CoNiCrAlY coatings exhibit higher porosity compared to HVOF coatings, resulting in faster TGO layer growth despite the lower oxide content (Ref 7). HVOF spraying of fine-grained materials can increase particle oxidation due to larger specific surfaces (Ref 8). Al depletion at the TGO/CoNiCrAlY interface in HVOF-sprayed coatings does not cause chemical failure (Ref 9). Comparatively, as-sprayed CGS and HVOF coatings share similar microstructures, while APS coatings have higher porosity and oxide content. Minimal oxide growth rates are observed for HVOF coatings, closely followed by CGS coatings (Ref 3).

The activated-combustion-high velocity air-fuel process (AC-HVAF) offers the advantage of moderate particle temperature and high particle velocity, enabling control over oxidation and microstructure of the MCrAlY coating for improved functionality. Additionally, its high efficiency contributes to better resource utilization. However, the lack of fundamental understanding of the flow and combustion processes prevents the HVAF process from being widely used. In most studies, only the observed coating qualities are described and analyzed. The relationship between the observed phenomena and the process is rarely investigated.

## Related Works

AC-HVAF process is a combination of various physical and chemical phenomena, involving turbulent flow, combustion, heat transfer, and compressible gas flow. Introducing the powders into the process initiates heat and momentum transfer between the gas stream and the particles. Simulation, particularly computational fluid dynamics (CFD), has proven to be a powerful tool for analyzing

thermal spray processes, including gas dynamics and in-flight particle behavior. Three-dimensional CFD modeling of HVAF process is developed to simulate the flight process of Fe-based amorphous alloy particles considering the catalytic ceramic as inlet for the air-propane mixture. The nitrogen flow rate and particle size were studied on their influence on their in-flight characteristics (Ref 10). Similar simulation was carried out taking into account the ceramic disk and the radial inlets for the compressed air (Ref 11). The effects of different fuel types and process parameters on the performance of AC-HVAF were studied in two-dimensional CFD simulations (Ref 12) followed by further investigations on different air-propane ratios and nozzle geometries (Ref 13). Two-dimensional CFD gas-solid coupling model is also developed to study the flight behavior of titanium alloy powder particles during HVAF spraying. On this basis, the discrete phase model (DPM) of titanium particles was carried out by the Lagrangian method to determine the particle flight behavior (Ref 14). With addition of process diagnostics, HVAF spray parameters for fabricating CoNiCrAlY coatings were developed based on detailed process analyses to characterize the working gas jet and the particles in-flight and calculate the gas velocities (Ref 15).

Numerical simulations of the AC-HVAF process that can be found in the literature are often modeled with simplifications, either two-dimensional or without taking into account the technical details of the spray gun system. The mixing process of air and propane in the mixing chamber was not considered in most studies. In addition, the compressed air flowing into the combustion chamber is given by the mass flow rate in most numerical models. However, in most AC-HVAF systems, the mass flow of compressed air is controlled by the inlet pressure and is distributed both for combustion and as a cooling medium for the spray gun. This detail is not found in the existing models. Therefore, a complete simulation model of the AC-HVAF process is developed as part of this study. The model includes the three-dimensional modeling of the spray gun up to the free-jet region, the mixing process in the mixing chamber and the distribution of compressed air as an oxidizing agent in the combustion chamber and as a cooling medium for the entire spray gun.

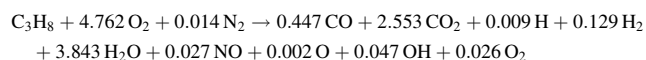
The objective of this study is to manufacture a CoNiCrAlY coating with reduced porosity and oxide content using the AC-HVAF process. The process parameters are established through CFD simulation, building upon prior research (Ref 16). The simulation model is utilized to investigate the influence of the process parameters on the particle in-flight properties. Additionally,  $\text{H}_2$  is introduced into the numerical model as a secondary carrier gas to the primary carrier gas  $\text{N}_2$ . The simulation model of AC-HVAF process is subsequently validated against the

measured particle velocities. Finally, the microstructure of the coatings fabricated with the process parameters determined from the simulation is analyzed. The coating parameters include variations in coarse and fine powder fractions, carrier gas compositions, and stand-off distances. The experimental results complement the simulated particle in-flight properties and enhance the understanding of AC-HVAF.

**Model Description**

CFD simulations of AK-07 AC-HVAF thermal spray gun (Kermetico, Inc., Benicia, USA) were conducted using Ansys Fluent 2021 R2 (ANSYS, Inc., Canonsburg, USA). The simulation model allows the calculation of particle temperature and velocity upon impact onto the substrate, which is significant for the resulting coating microstructure.

A three-dimensional CFD simulation model of AK-07 was developed to investigate the correlation between the process parameters and the in-flight behavior of CoNiCrAlY particles, for details, refer to (Ref 16). Built upon the previous work, the model has been modified from a longer nozzle #4L with length of 225 mm to a shorter nozzle #2L with length of 150 mm, which is more suitable for application of metallic materials. Moreover, H<sub>2</sub> as secondary carrier gas is introduced. The flow dynamic model is modeled with  $k-\omega$ -shear stress transport turbulent model. The combustion modeling relies upon the eddy dissipation model with following chemical combustion reaction (Ref 17):



To simulate the interaction between the gas stream and the particles, a discrete phase model with a two-way coupling method is applied to account for the interaction between the gas stream and the powders. The drag force is the major force acting on the particles and can be described as follows:

$$F_D = C_D \cdot A_p \cdot \rho_g \cdot |v_p - v_g| \cdot (v_g - v_p) / 2$$

In this study, the relationship between the drag coefficient  $C_D$  and particle Reynolds number  $Re_p$  is calculated using the approach of Vardelle et al. (Ref 18):

$$C_D = \begin{cases} 24/Re_p & Re_p \leq 0.2 \\ 24 \cdot (1 + 0.1 \cdot Re_p^{0.99})/Re_p & 0.2 < Re_p < 2 \\ 24 \cdot (1 + 0.11 \cdot Re_p^{0.81})/Re_p & 2 < Re_p < 21 \\ 24 \cdot (1 + 0.189 \cdot Re_p^{0.62})/Re_p & 21 < Re_p \leq 500 \\ 0.44 & 500 < Re_p \end{cases}$$

The convective heat transfer between the gas mixture and the particles is written as follows:

$$h = k_g \cdot Nu_p / d_p$$

The particle Nusselt number is based on the Hughmark correlation as follows (Ref 19):

$$Nu_p = \begin{cases} 2 + 0.60 \cdot Re_p^{0.5} \cdot Pr_g^{0.33} & 0 \leq Re_p < 776.06 \text{ und } 0 \leq Pr_g < 250 \\ 2 + 0.27 \cdot Re_p^{0.62} \cdot Pr_g^{0.33} & 776.06 < Re_p \text{ und } 0 \leq Pr_g < 250 \end{cases}$$

The simulation domain is depicted in Fig. 1, and the material properties of CoNiCrAlY are taken from the previous work (Ref 16). The investigated process parameters are listed in Table 1 in the next section.

Following a thorough mesh convergence study, the current mesh setup for the simulation model employs element sizes of 1.6 mm for the combustion chamber, 1.6 mm for the nozzle, and 0.8 mm for the core region of the free-jet with a total of 4,143,856 cells.

**Experimental Procedure**

The experiments were conducted using an AC-HVAF-System AK-07 equipped with combustion chamber #3 with an internal diameter of 70 mm and a de Laval nozzle with a length of 150 mm and expansion diameter of 17.2 mm. Commercially available CoNiCrAlY powders (Oerlikon Metco Europe GmbH, Kelsterbach, Germany) Amdry 9954 with powder fraction of  $-63 + 11 \mu m$  in the manuscript will be referred as coarse powder, and Amdry 9951 with powder fraction of  $-38 + 5.5 \mu m$ , as fine powder, were deposited on mild steel substrate. The Morphologi G2 optical particle analyzer (Malvern Instruments GmbH, Herrenberg, Germany) is used to determine the actual particle size distribution. Figure 2 shows the images of the powders, the volumetric frequency distribution of the measured particles with  $d_{50} = 17 \mu m$  for the fine powder and  $d_{50} = 28 \mu m$  for the coarse powder, and the applied Rosin-Rammler distribution of the particles in the simulation.

The simulation model is employed to study the influence of carrier gas compositions and stand-off distances on the particle in-flight properties. The parameters for the spray gun, such as the pressure of the compressed air and propane as well as the volume flow rate of the primary carrier gas N<sub>2</sub>, are listed in Table 1. Based on the simulation results of the particle velocities and the flow field, which are discussed in the next section, a suitable parameter window for coarse and fine powder can be identified. The investigated coating parameters are listed in Table 1. For validating the simulation results, particle in-flight properties such as particle temperatures and velocities were measured using SprayWatch 4S (Oseir Ltd., Tampere, Finland).

**Fig. 1** Simulation domain of the AC-HVAF process

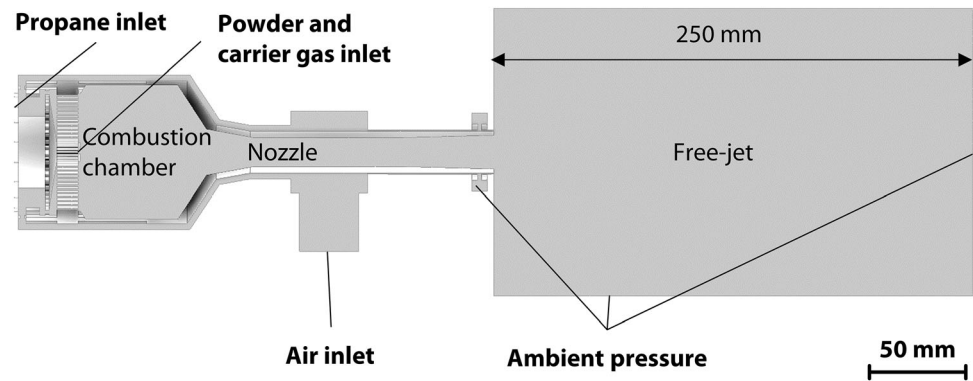


**Table 1** Process parameters for fabrication of the coatings

Process parameters	Unit	Value	
<i>Spray gun parameter</i>			
Compressed air	MPa	0.62	
Propane	MPa	0.55	
Nitrogen	SLPM	25	
Powder feed rate of coarse powder	rpm	$2.5 \pm 39$ g/min	
Powder feed rate of fine powder	rpm	$2.5 \pm 24$ g/min	
Parameter	Powder fraction, $\mu\text{m}$	Hydrogen	Stand-off distance $d_s$ , mm
<i>Variation of powder sizes, carrier gas mixtures and stand-off distances</i>			
C-N-200	– 63 + 11	–	200
C-H-200	– 63 + 11	29 SLPM	200
C-N-250	– 63 + 11	–	250
C-H-250	– 63 + 11	29 SLPM	250
F-N-200	– 38 + 5.5	–	200
F-H-200	– 38 + 5.5	29 SLPM	200
F-N-250	– 38 + 5.5	–	250
F-H-250	– 38 + 5.5	29 SLPM	250

To enhance understanding of how particle in-flight properties affect the deposited coatings, the microstructures of the coatings were analyzed. All coatings are fabricated over 20 passes. Scanning electron microscopy (SEM) Phenom XL (Thermo Fisher Scientific Inc., Massachusetts, USA) with energy dispersed spectroscopy (EDS) was utilized for this analysis. The phases in the coatings were examined using x-ray diffraction (XRD) by XRD 3000 (GE Energy Germany, Ratingen, Germany) in a range from  $20^\circ \leq 2\theta \leq 80^\circ$ , employing a Cu-K $\alpha$  radiation source with a step size of  $0.02^\circ$  and step time of 5 s. Additionally, surface topology and surface roughness of the coatings were assessed using a confocal laser scanning microscope

VK-X200 (Keyence Deutschland GmbH, Neu-Isenburg, Germany).

## Results and Discussion

### Simulation Results

The simulation model was set up in two phases: initially representing only the gas flow without powder injection, crucial for understanding HVAF process flow properties. Figure 3 displays the simulated temperature and velocity flow field in a steady state. The asymmetric temperature distribution within the combustion chamber is likely attributed to minor differences in the mass fraction of the propane–air–gas mixtures exiting the mixing chamber. Despite the use of a shorter nozzle in the AK-07 AC-HVAF system, a relatively high flame jet velocity is observed, reaching just under 1500 m/s, indicating a supersonic state with  $Ma > 2$ . The core region of the flame jet dissipates after approximately 165 mm, followed by a rapid decrease in gas flow velocity and temperature.

Subsequently, the simulation involved injecting powder particles to analyze their in-flight properties. The influence of the carrier gas composition on these properties was examined both numerically and experimentally. To validate the simulation results, the particle in-flight properties were measured at stand-off distances of  $d_s = 100$  mm,  $d_s = 200$  mm, and  $d_s = 250$  mm using SprayWatch 4S. Figure 4 illustrates the calculated and measured particle properties for coarse powder at given stand-off distances. The  $d_{\min}$ ,  $d_{50}$ , and  $d_{\max}$  of the coarse powder are 11, 28, and 63  $\mu\text{m}$ , respectively. The measured particle velocity corresponds to the calculated particle velocity for the particle diameter  $d_{\min}$ . The addition of  $\text{H}_2$  as a secondary carrier gas had no significant impact on particle velocity, as confirmed by experimental measurements. However, there was a noticeable decrease of approximately  $\Delta T \approx 100$  K in particle temperature due to the presence of  $\text{H}_2$ . The measured particle temperature refers to the surface

**Fig. 2** Characterization of CoNiCrAlY powders: (a) SEM images, (b) particle size distribution, and (c) Rosin–Rammler distribution adopted for the simulations

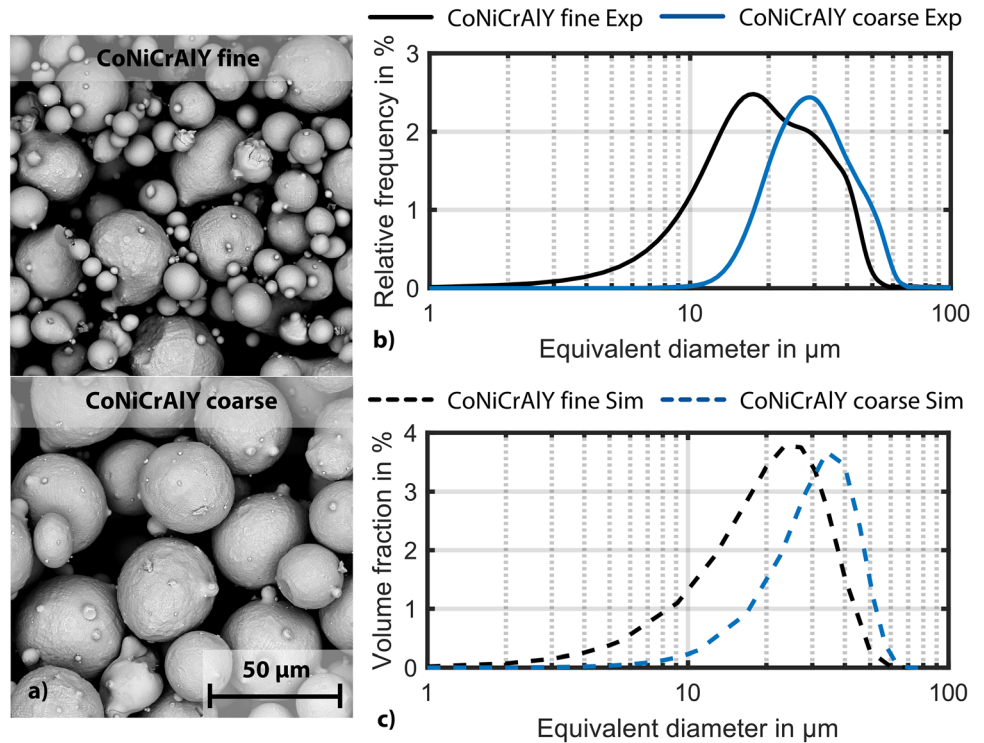


**Fig. 3** Simulated temperature and velocity flow field of AK-07 AC-HVAF system

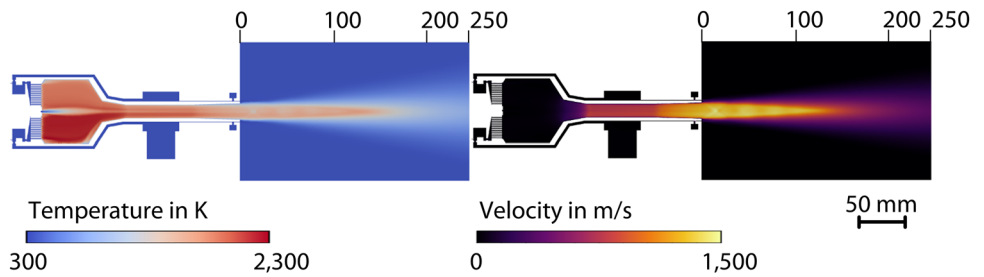
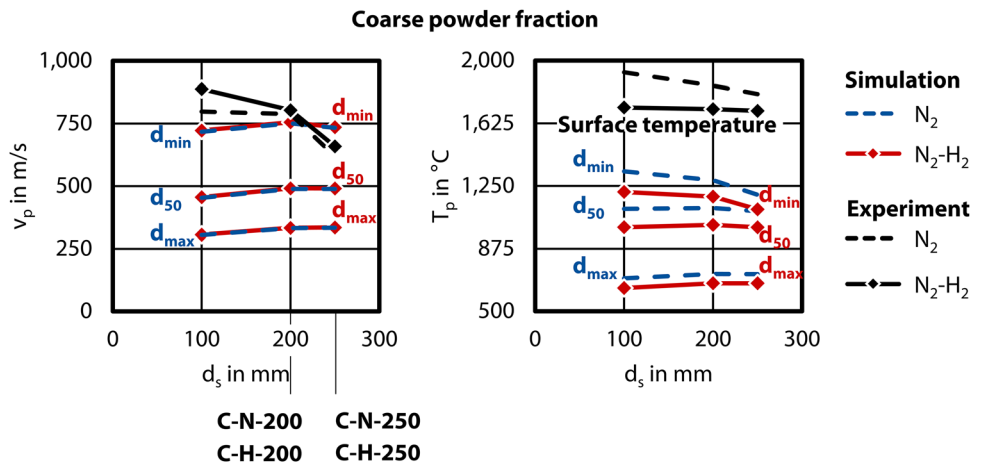


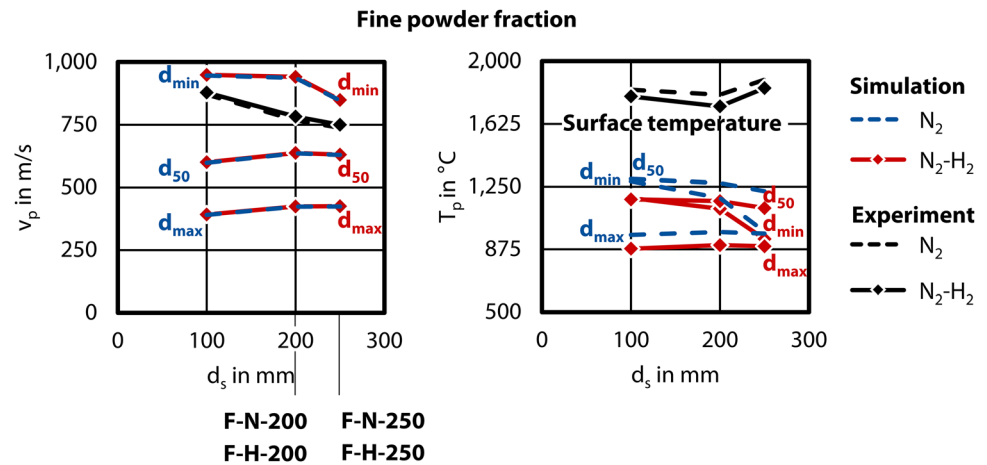
**Fig. 4** Calculated and measured particle velocity and temperature of coarse CoNiCrAlY powder with different carrier gas compositions



temperature. The diagnostic system tends to detect finer particles due to the short exposure time and the incandescent particles. In the simulation, the powder particle is defined as a point mass with the resulting calculated

particle temperature representing the bulk temperature due to the implemented lumped capacitance method. In addition, the SprayWatch 4S particle diagnostic system’s limitation in detecting particle temperatures above

**Fig. 5** Calculated and measured particle velocity and temperature of fine CoNiCrAlY powder with different carrier gas compositions



$T > 1000$  °C prevented the measurement of coarser particle temperatures. The coating microstructure further supported this difference, showing semi-molten particles and indicating that the measured temperature was the surface temperature of the finer particles.

Figure 5 displays the calculated and measured particle in-flight properties of fine powder at various stand-off distances of  $d_s = 100$  mm,  $d_s = 200$  mm, and  $d_s = 250$  mm. The  $d_{min}$ ,  $d_{50}$ , and  $d_{max}$  of the fine powder are 5.5, 17, and 38  $\mu\text{m}$ , respectively. The measured particle velocity is within the range of the calculated particle velocities of the particle diameters  $d_{min}$  and  $d_{50}$ . As for the particle temperature, finer particles cool down faster compared to coarser particles due to their higher Reynolds numbers. This phenomenon can be captured in the simulation. The use of  $\text{N}_2\text{-H}_2$  as a carrier gas results in a lower particle surface temperature, similar to the coarse powder behavior.

Based on the results of the numerically and experimentally determined particle velocities, and the gas dynamic flow field, a suitable parameter window for the fabrication of the coatings could be identified. While the particles have a high velocity at  $d_s < 200$  mm, the core region of the flame is at a high temperature up to approx. 165 mm after the nozzle outlet. Therefore, the stand-off distances  $d_s = 200$  mm and  $d_s = 250$  mm were selected to manufacture the coatings with both powder fractions. In addition, the variation of the carrier gas composition due to the observed particle temperature differences is included in the parameter variation.

### Examination of Coating Microstructure

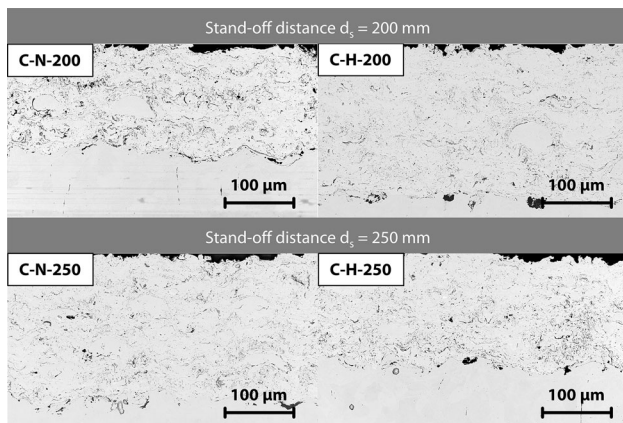
Coating microstructure analysis is crucial for assessing the quality of fabricated coatings, particularly regarding porosity and oxide content in MCrAlY. The percentage area porosity was automatically calculated by digital image

analysis using ImageJ software (National Institutes of Health, USA) by determining the black areas in the SEM microstructure images of 3 images for each coating parameter. The oxide content in wt. % was qualitatively measured by EDS elemental mapping analysis.

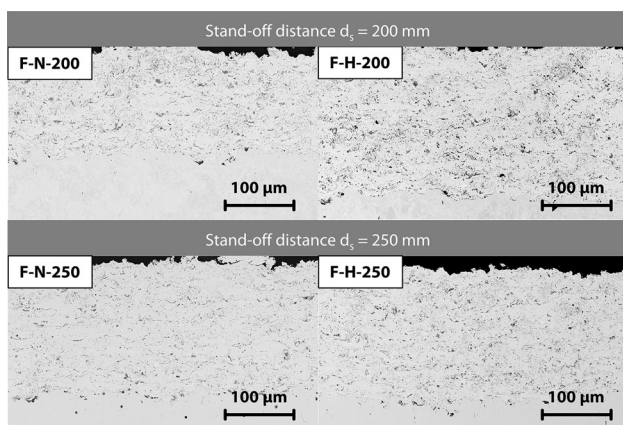
Figure 6 displays cross sections of CoNiCrAlY coating microstructure with coarse powder. Coating thickness for parameters C-N-200, C-H-200, C-N-250, and C-H-250 is 158, 233, 198, and 162  $\mu\text{m}$ , respectively. The coating with  $\text{N}_2\text{-H}_2$  as carrier gas at a stand-off distance of  $d_s = 200$  mm, C-H-200, shows the highest deposition rate within the investigated parameters. The cross sections reveal nearly spherical semi-molten particles. All coatings with coarse powder have a low porosity of  $\Phi < 0.6\%$  and relatively low oxide content ranging from 2.1 to 2.7 wt.%.

Figure 7 illustrates cross sections of CoNiCrAlY coating microstructure with fine powder. Coating thickness for parameters F-N-200, F-H-200, F-N-250, and F-H-250 is 182, 220, 203, and 204  $\mu\text{m}$ , respectively. Similar to the coatings with coarse powder, the coating with  $\text{N}_2\text{-H}_2$  as carrier gas at a stand-off distance of  $d_s = 200$  mm, F-H-200, shows the highest deposition rate within the investigated parameters. Coatings with fine powder exhibit fewer semi-molten particles, resulting in a very low porosity of  $\Phi < 0.4\%$ . However, they exhibit higher oxide content compared to coatings with coarse powder, with oxides, which are shown as darker areas in the cross sections, distributed homogeneously throughout the coatings. The oxide content is ranging from 2.7 to 3.0 wt.%.

Figure 8 shows SEM images of CoNiCrAlY coating with parameter C-H-200 and F-H-200, captured using backscattered electron detector and topography mode to depict coating density. The observed microstructure appears very dense with minimal porosities. Topography mode images reveal oxides characterized by emerging surfaces. In the EDS elemental mapping analysis, the observed element O overlaps with the element Al, as



**Fig. 6** Cross section of CoNiCrAlY coatings with coarse powder



**Fig. 7** Cross section of CoNiCrAlY coatings with fine powder

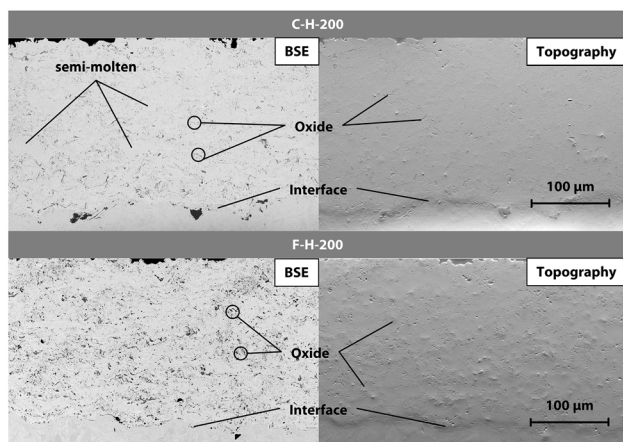


**Fig. 8** SEM cross section image of CoNiCrAlY coatings with BSE and topography modes

shown in Fig. 9. The comparison of the porosity and the oxide content of the investigated parameters is displayed in Fig. 10.

### XRD Analysis

Figure 11 shows the XRD patterns of the CoNiCrAlY feedstock powders and as-sprayed coatings. The feedstock powder contains  $\gamma$ -matrix and  $\beta$ -(Co,Ni)Al phases, while the as-sprayed coatings show indistinct  $\beta$ -phase peaks. Broadening of  $\gamma$ -matrix phase peaks indicates grain refinement and micro-stress from severe plastic deformation during deposition, which also found in as-sprayed cold gas CoNiCrAlY coatings (Ref 20). XRD analysis was not able to detect obvious oxide phases in coatings with fine powder.

### Evaluation of Surface Roughness and Coating Surface Topology

Bond coats for TBC systems require a specific threshold of surface roughness to ensure proper coating adherence. The surface roughness depends on the manufacturing process, particle size, and stand-off distance. The cross section analysis of coatings provides insights into microstructure, porosity, and oxides. On the other hand, coating topology reveals the impact behavior of coarse and fine powder particles, which is relevant for the surface roughness of the coatings. Coarse particles appear partially molten with some spherical shapes, as shown in Fig. 12. In contrast, fine particles, which are mostly molten upon impact, resulting in disk-shaped splats with splashes.

By means of confocal laser scanning microscopy it is possible to determine surface topology of coatings over a greater area. Three-dimensional surface images in Fig. 13 highlight the distinct roughness of coarse and fine coating samples. Coarse particles are evident as denser gold-colored regions with elevated contours in the topology contour, displaying larger diameters. It is also observable that with increasing stand-off distance and finer particles, the gold-colored regions become less due to the molten splats, resulting in lower surface roughness.

Comparison of surface roughness of CoNiCrAlY coatings with various process parameters is shown in Fig. 14. It shows that coatings with coarse powder led to a higher surface roughness due to the semi-molten particles previously mentioned. When coating with fine and coarse powders, increasing the stand-off distance results in lower surface roughness, as the higher kinetic energy of the coarse fraction of the powders used during particle deposition provides deformation of the particles. Nevertheless, the average surface roughness of the coated samples with coarse CoNiCrAlY powder is in the desired range of 6–9  $\mu\text{m}$  for a bond coat. For the coatings with fine CoNiCrAlY powder, the surface roughness is between 5 and 7  $\mu\text{m}$ .

**Fig. 9** Exemplary EDS elemental analysis of CoNiCrAlY coating with coarse powder

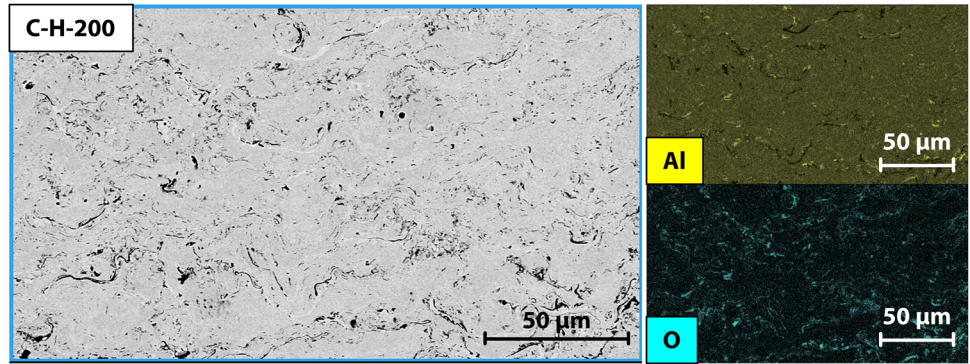


**Fig. 10** Comparison of the porosity and oxide content of various process parameters

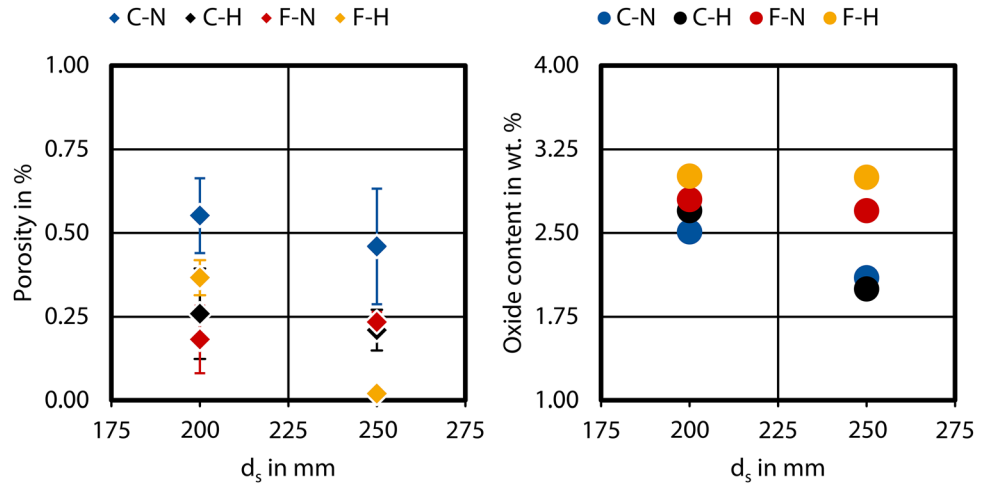
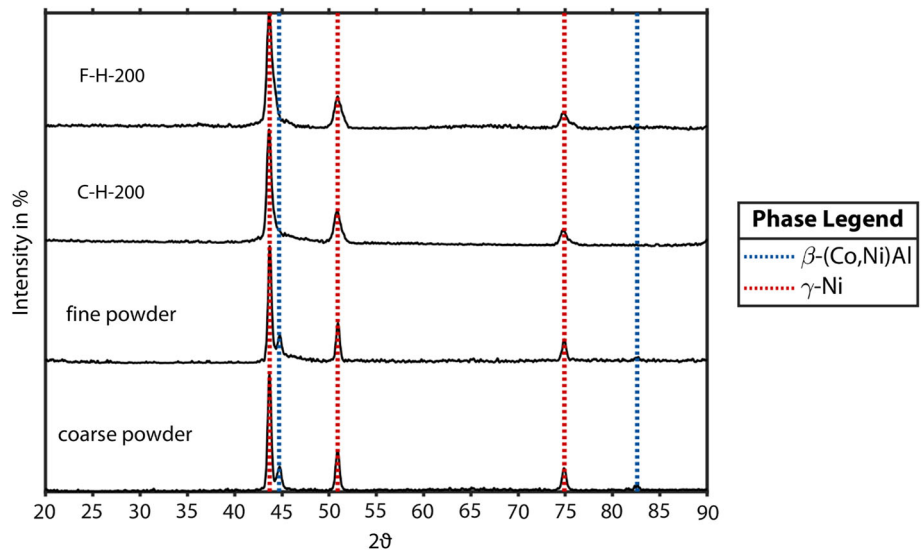


**Fig. 11** XRD patterns of feedstock powders and as-sprayed coatings



**Conclusion**

The AC-HVAF process, which is characterized by a moderate particle temperature and high particle velocity, enables the production of coatings with low oxidation and porosity. However, the limited understanding of the flow

and combustion processes hinders its wide application. Numerical models such as CFD simulations are often used to solve this challenge. However, modeling of the AC-HVAF process often involves simplifications, either two-dimensional or without considering the technical details of the spray gun system. Therefore, a complete simulation



**Fig. 12** Surface morphology of CoNiCrAlY coatings with coarse and fine powder

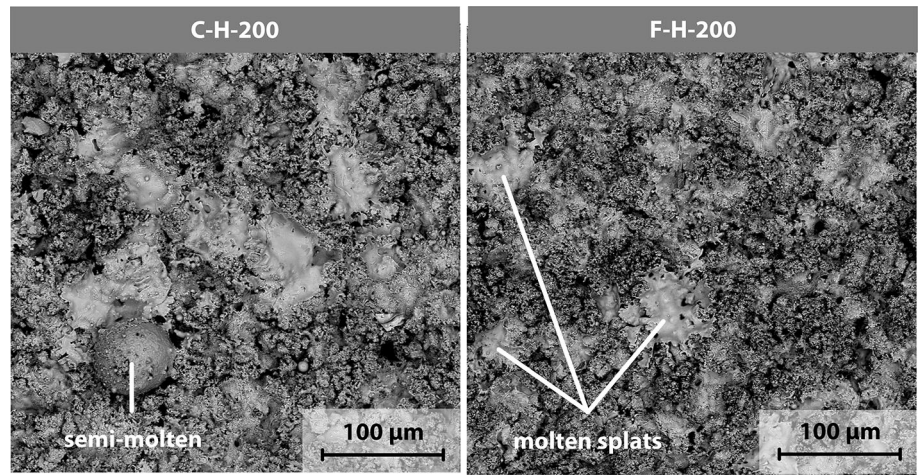


**Fig. 13** Three-dimensional surface topology of CoNiCrAlY coatings fabricated by HVOF spraying

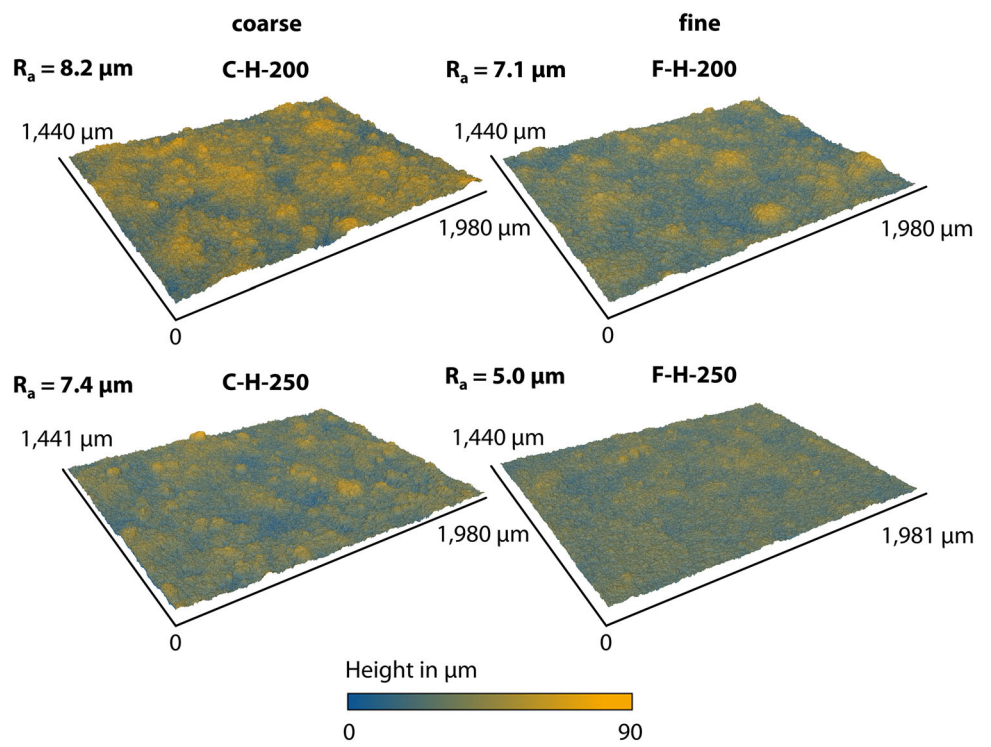
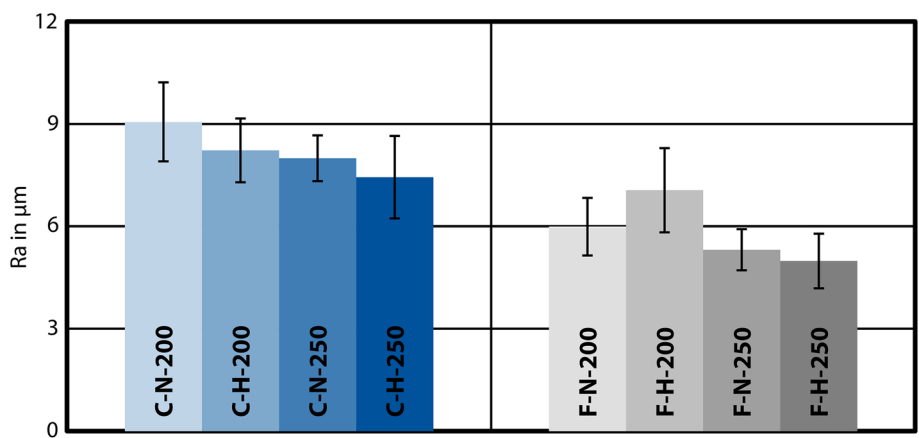


**Fig. 14** Comparison of the surface roughness of various process parameters



model including the mixing chamber and the distribution of compressed air as oxidizing agent and cooling medium was developed and utilized within the present investigation to predict suitable parameters for both investigated powder fractions. The predicted process parameters were supported with experiments that provide valuable insights into various aspects that influence the microstructure of CoNiCrAlY coatings, such as porosity and oxide content. In particular, observations have been made on the effects of modifying carrier gases by introducing H<sub>2</sub> as a secondary carrier gas on particle temperature and velocity, as well as on variations in coating thickness. These parameters, together with the powder particle size, contribute to the understanding of the coating roughness and surface topology. The following significant results can be derived from the study:

1. The simulation model can determine a suitable process parameter window for commercially available powder fractions for fabricating low porosity and low oxide CoNiCrAlY coatings by HVAF spraying.
2. The carrier gas composition N<sub>2</sub>–H<sub>2</sub> affects the temperatures of the particles in-flight, with H<sub>2</sub> leading to lower particle temperatures. The particle velocity remains unaffected by the variation of the carrier gas composition.
3. H<sub>2</sub> as an additional carrier gas leads to higher coating thickness when spraying at stand-off distance of  $d_s = 200$  mm. However, the effect is not noticeable at greater stand-off distance.
4. CoNiCrAlY coatings with low porosity could be achieved with commercially available coarse and fine powder by HVAF spraying. Coatings with coarse powder have lower oxide content, which determined qualitatively by EDS elemental analysis.
5. Surface roughness is affected by stand-off distance and particle size. Lower stand-off distance in combination with coarse particles increases the surface roughness due to the higher kinetic energy and semi-molten particles, respectively.

Overall, very dense coatings with low oxide content and suitable roughness value for a bond coat were successfully manufactured using the process parameters predicted from the simulation. The analysis of the coating microstructure complements the findings from the simulation on the particle in-flight properties. In future work, the simulation model needs to be developed further to enable the prediction of the particle surface temperature by discretizing the powder particles. This allows the degree of oxidation of the particles in-flight to be determined. Consequently, the process parameters can be optimized to reduce oxidation. In addition, free-standing CoNiCrAlY coatings with the studied parameters will be fabricated and a precise

quantification of the oxygen content of these coatings will be performed by means of carrier gas hot extraction. Moreover, CoNiCrAlY coatings with the currently studied parameters will be coated on Inconel 718 samples and subjected to oxidation tests. The oxide growth rates of the sprayed and vacuum annealed coatings will be investigated.

**Acknowledgments** This work was based on the DFG project “Simulationsunterstützte Prozessentwicklung für die Applikation von MCrAlY-Beschichtungen mittels des AC-HVAF-Prozesses” BO 1979/75-1, 437084607. The authors gratefully acknowledge the financial support of the German Research Foundation (DFG). Simulations were performed with computing resources granted by RWTH Aachen University under project rwth0723. The authors would like to thank Atharva Wagh for his valuable support in evaluating the simulation results and the experimental measurements.

**Funding** Open Access funding enabled and organized by Projekt DEAL.

**Open Access** This article is licensed under a Creative Commons Attribution 4.0 International License, which permits use, sharing, adaptation, distribution and reproduction in any medium or format, as long as you give appropriate credit to the original author(s) and the source, provide a link to the Creative Commons licence, and indicate if changes were made. The images or other third party material in this article are included in the article’s Creative Commons licence, unless indicated otherwise in a credit line to the material. If material is not included in the article’s Creative Commons licence and your intended use is not permitted by statutory regulation or exceeds the permitted use, you will need to obtain permission directly from the copyright holder. To view a copy of this licence, visit <http://creativecommons.org/licenses/by/4.0/>.

## References

1. T. Mori, S. Kuroda, H. Murakami, H. Katanoda, Y. Sakamoto, and S. Newman, Effects of initial oxidation on  $\beta$  phase depletion and oxidation of CoNiCrAlY bond coatings fabricated by warm spray and HVOF processes, *Surf. Coat. Technol.*, 2013, **221**, p 59-69.
2. D. Naumenko, R. Pillai, A. Chyrkin, and W.J. Quadackers, Overview on recent developments of bondcoats for plasma-sprayed thermal barrier coatings, *J. Therm. Spray Technol.*, 2017, **26**(8), p 1743-1757.
3. P. Richer, M. Yandouzi, L. Beauvais, and B. Jodoin, Oxidation behaviour of CoNiCrAlY bond coats produced by plasma, HVOF and cold gas dynamic spraying, *Surf. Coat. Technol.*, 2010, **204**(24), p 3962-3974.
4. T. Koomparking, S. Damrongrat, and P. Niranatlumpong, Al-rich precipitation in CoNiCrAlY bondcoat at high temperature, *J. Therm. Spray Technol.*, 2005, **14**(2), p 264-267.
5. G. Mauer, D. Sebold, and R. Vaßen, MCrAlY bondcoats by high-velocity atmospheric plasma spraying, *J. Therm. Spray Technol.*, 2014, **23**(1), p 140-146.
6. F.R. Caliari, F.S. Miranda, D.A.P. Reis, A.M. Essiptchouk, and G.P. Filho, Supersonic plasma spray deposition of CoNiCrAlY coatings on Ti-6Al-4V alloy, *J. Therm. Spray Technol.*, 2017, **26**(5), p 880-889.

7. W.R. Chen, E. Irissou, X. Wu, J.-G. Legoux, and B.R. Marple, The oxidation behavior of TBC with cold spray CoNiCrAlY bond coat, *J. Therm. Spray Technol.*, 2011, **20**(1), p 132-138.
8. C.-J. Li and W.-Y. Li, Effect of sprayed powder particle size on the oxidation behavior of MCrAlY materials during high velocity oxygen-fuel deposition, *Surf. Coat. Technol.*, 2003, **162**(1), p 31-41.
9. W.R. Chen, Degradation of a TBC with HVOF-CoNiCrAlY bond coat, *J. Therm. Spray Technol.*, 2014, **23**(5), p 876-884.
10. H.-R. Jiang, M.-L. Li, X.-S. Wei, T.-C. Ma, Y. Dong, C.-X. Ying, Z.-Y. Liao, and J. Shen, Numerical investigation of in-flight behavior of Fe-based amorphous alloy particles in AC-HVAF thermal spray process, *J. Therm. Spray Technol.*, 2019, **28**(6), p 1146-1159.
11. F. Liu, Z. Li, M. Fang, and H. Hou, Numerical analysis of the activated combustion high-velocity air-fuel spraying process: a three-dimensional simulation with improved gas mixing and combustion mode, *Materials*, 2021, **14**(3), p 657.
12. X. Gao, C. Li, Y. Xu, X. Chen, and X. Han, Effects of fuel types and process parameters on the performance of an activated combustion high velocity air-fuel (AC-HVAF) thermal spray system, *J. Therm. Spray Technol.*, 2021, **30**(7), p 1875-1890.
13. X. Gao, C. Li, D. Zhang, H. Gao, and X. Han, Numerical analysis of the activated combustion high-velocity air-fuel (AC-HVAF) thermal spray process: a survey on the parameters of operation and nozzle geometry, *Surf. Coat. Technol.*, 2021, **405**, p 126588.
14. X. Han, C. Li, X. Gao, X. Chen, and Z. Liu, Numerical study on the behavior of titanium particles in the process of warm spraying, *Weld. World*, 2022, **66**(7), p 1305-1314.
15. G. Mauer, K.-H. Rauwald, and R. Vaßen, The potential of high velocity air fuel spraying (HVAF) to manufacture bond coats in thermal barrier coating systems, in: *Thermal Spray 2023: Proceedings from the International Thermal Spray Conference* (2023), pp. 625-632.
16. K. Bobzin, H. Heinemann, and K. Jasutyn, Correlation between process parameters and particle in-flight behavior in AC-HVAF, *J. Therm. Spray Technol.*, 2023, **32**(2), p 559-567.
17. S. Gordon and B.J. McBride, Computer program for calculation of complex chemical equilibrium compositions, rocket performance, incident and reflected shocks, and Chapman-Jouguet detonations. Scientific and Technical Information Office National Aeronautics and Space Administration; [for sale by the National Technical Information Service Springfield Va.] (1971)
18. M. Vardelle, A. Vardelle, P. Fauchais, and M.I. Boulos, Plasma—particle momentum and heat transfer: modelling and measurements, *AIChE J.*, 1983, **29**(2), p 236-243.
19. G.A. Hughmark, Mass and heat transfer from rigid spheres, *AIChE J.*, 1967, **13**(6), p 1219-1221.
20. P. Richer, A. Zúñiga, M. Yandouzi, and B. Jodoin, Conicrally microstructural changes induced during cold gas dynamic spraying, *Surf. Coat. Technol.*, 2008, **203**(3), p 364-371.

**Publisher's Note** Springer Nature remains neutral with regard to jurisdictional claims in published maps and institutional affiliations.